VCP and PSMF1: antagonistic regulators of proteasome activity

Christoph S. Clemen[1),*], Marija Marko[1)], Karl-Heinz Strucksberg[1)], Juliane Behrens[1)], Linda Gärtner[2)], Lilli Winter[3)], Frederic Chevessier[3)], Matthias Türk[4)], Karthikeyan Tangavelou[1)], Johanna Schütz[3)], Jan Matthias[1)], Karsten Klopffleisch[5)], Franz-Georg Hanisch[6)], Wolfgang Rottbauer[2)], Ingmar Blümcke[3)], Steffen Just[2)], Ludwig Eichinger[1)], Andreas Hofmann[7),8)], Rolf Schröder[3),*]

[1)] Institute of Biochemistry I, Medical Faculty, University of Cologne, Joseph-Stelzmann-Str. 52, 50931 Cologne, Germany
[2)] Molecular Cardiology, Department of Internal Medicine II, University Hospital Ulm, Albert-Einstein-Allee 23, 89081 Ulm, Germany
[3)] Institute of Neuropathology, University Hospital Erlangen, Schwabachanlage 6, 91054 Erlangen, Germany
[4)] Department of Neurology, University Hospital Erlangen, Schwabachanlage 6, 91054 Erlangen, Germany
[5)] Institute of Genetics, University of Cologne, Zülpicher Str. 47a, 50674 Cologne, Germany
[6)] Institute of Biochemistry II, Medical Faculty, and Center for Molecular Medicine Cologne, University of Cologne, Robert-Koch-Str. 21, 50931 Cologne, Germany
[7)] Structural Chemistry Program, Eskitis Institute, Griffith University, N75 Don Young Road, Nathan, Queensland 4111, Australia
[8)] Faculty of Veterinary Science, The University of Melbourne, Parkville, Victoria 3030, Australia

*Authors for correspondence:
Christoph S. Clemen, Institute of Biochemistry I, Medical Faculty, University of Cologne, Joseph-Stelzmann-Str. 52, 50931 Cologne, Germany; phone: +49 221 478 6987; fax: +49 221 478 6979; e-mail: christoph.clemen@uni-koeln.de
Rolf Schröder, Institute of Neuropathology, University Hospital Erlangen, Schwabachanlage 6, 91054 Erlangen, Germany; phone: +49 9131 85 34782; fax: +49 9131 85 26033; e-mail: rolf.schroeder@uk-erlangen.de

Abstract

Protein turnover and quality control by the proteasome is of paramount importance for cell homeostasis. Dysfunction of the proteasome is associated with ageing processes and human diseases such as neurodegeneration, cardiomyopathy, and cancer. The regulation of activation and inhibition of this fundamentally important protein degradation system remains largely unresolved. We demonstrate that the evolutionarily highly conserved type II AAA ATPase VCP and the proteasome inhibitor PSMF1/PI31 interact directly, and antagonistically regulate proteasomal activity. Our data provide novel insight into the regulation of proteasomal activity.

Key words

proteasome; protein quality control; VCP; p97; triple-A ATPase; PSMF1; proteasome inhibitor PI31; mouse model; *Dictyostelium discoideum*

Introduction

Homeostasis of cells is highly dependent on the integrity of the proteasome, which hydrolyses intracellular proteins into small peptides, thus regulating protein turnover and removal of misfolded and poly-ubiquitinated proteins (Jung et al, 2009; Sorokin et al, 2009). Proteasome dysfunction has been implicated in a wide variety of human diseases including neurodegenerative disorders, muscular dystrophies, cardiomyopathies, immune defects, metabolic diseases, and cancer (Gomes, 2013; Jankowska et al, 2013).

The 20S core of the proteasome is a 700 kDa barrel-shaped structure composed of four stacked rings. The two outer rings are formed by seven different α-

subunits (PSMA1-7 in mammals) that function as entry sites, whereas the two inner rings, which consist of seven different β-subunits (PSMB1-7), exert the trypsin-, chymotrypsin-, and caspase-like proteolytic activities. Regulation of the proteasome is a complex and mainly unresolved issue. Activation of the 20S core under physiological conditions requires binding of the 19S regulatory particle (synonym PA700) to one of the outer rings leading to the formation of the functionally active 26S proteasome. Alternatively, the 20S core can be activated by other components such as the PA28α/β hetero- and PA28γ multimers (11S complexes), and the PA200 (PSME4) monomer (Dahlmann, 2005; Jung et al, 2009; Rechsteiner & Hill, 2005; Sorokin et al, 2009).

VCP (valosin containing protein; orthologs known as VAT, CDC48, CdcD, TER94, p97) is a ubiquitously expressed and evolutionarily highly conserved type II triple-A ATPase involved in a wide variety of essential cellular processes comprising nuclear envelope reconstruction, the cell cycle, post-mitotic Golgi reassembly, suppression of apoptosis, DNA damage response, and protein quality control mechanisms (Baek et al, 2013). The essential role of VCP in humans is highlighted by the observation that point mutations of the VCP gene cause three autosomal dominant disorders, namely IBMPFD (inclusion body myopathy with early onset Paget's disease of bone and frontotemporal dementia) (Watts et al, 2004), ALS14 (amyotrophic lateral sclerosis with or without frontotemporal dementia) (Johnson et al, 2010), and Hereditary Spastic Paraplegia (de Bot et al, 2012).

Here, we demonstrate that VCP and PSMF1 ~~directly~~ interact directly, and ~~antagonistically~~ regulate the activity of this fundamentally important protein degradation system in an antagonistic fashion.

Results

VCP directly interacts with the proteasome inhibitor PSMF1

To identify novel and disease relevant VCP binding partners, we have previouslyd performed VCP co-immunoprecipitation experiments, which resulted in the identification of PSMF1 as a putative candidate (supplementary tables 1 and 2 in (Clemen et al, 2010)). PSMF1 (proteasome inhibitor PI31 subunit (Chu-Ping et al, 1992)) is a highly conserved, proline-rich 31 kDa protein that inhibits the proteasomal activities by either direct binding to the outer rings of the 20S proteasome or competition with the activating particles for 20S binding (Cho-Park & Steller, 2013; McCutchen-Maloney et al, 2000; Zaiss et al, 1999).

By means of luminescence-based mammalian interactome mapping (Lumier) (Barrios-Rodiles et al, 2005), we investigated potential interactions of VCP with various target proteins. Using this novel experimental approach, which allows detection and quantitation of protein-protein interactions, we first confirmed VCP multimer formation (Fig. 1A) as well as interactions with the previously established VCP binding partners Ufd1 and Npl4. More importantly, we could demonstrate an interaction of VCP and PSMF1 within a similar dynamic range as observed for VCP and Ufd1 or Npl4 (Fig. 1B). Using pull-down assays employingwith purified recombinant proteins, we could demonstrate a direct interaction between VCP and its novel binding partner PSMF1 (Fig. 1C).

Reduced VCP levels cause decreased proteasomal activity

Previous studies showed that tThe targeted ablation of VCP in mouse, fruit fly, yeast, and the protist *Trypanosoma brucei* resultedis lethal in all these organisms in lethality (Frohlich et al, 1991; Lamb et al, 2001; Leon & McKearin, 1999; Müller et al, 2007). In VCP haploinsufficient mice (Fig. S1), which displayed a 30% and 40%

reduction of the VCP mRNA and protein levels, respectively (Fig. 2A-C), we noted an increase of poly-ubiquitinated proteins (Fig. 2C). Using a highly sensitive luminescence-based proteasomal activity assay, we studied the chymotrypsin-like activity in lower hind limb muscles derived from three months old mice. Here, the VCP haploinsufficient mice showed a significant reduction (32%) of the specific proteasomal activity as compared to wild-type littermates (Fig. 2D). The expression levels of 19S and 20S proteasome complexes as well as PSMF1 remained unchanged (Fig. 2C).

VCP and PSMF1 antagonistically regulate proteasome activity

To investigate potential roles of VCP and PSMF1 on proteasomal activity *in vitro*, we first added bacterially expressed, purified human VCP (100% sequence identity to murine VCP) to skeletal muscle lysates derived from the VCP haploinsufficient mice. This resulted in a dose-dependent increase of proteasomal activity (Fig. 3A). This effect, however, was not observed in analogous experiments using either purified human 26S or 20S proteasomes instead of the tissue lysate (Fig. 3B). The latter finding argues against a direct stimulatory effect of VCP on the proteasome and favors the presence of a co-factor in the tissue lysate.

We considered PSMF1 as a promising candidate and therefore used both purified VCP and PSMF1 proteins to analyze their activating and inhibiting effects on 20S proteasomal activity *in vitro* (Fig. 3C). Upon addition of VCP, the activity of purified proteasome remained unchanged (Fig. 3C, part i, red line), whileereas the addition of PSMF1 inhibited proteasomal activity as expected (part i, blue line). The subsequent addition of PSMF1 to the reaction already containing VCP significantly reduced the proteasomal activity (part ii, red line). Although the addition of VCP to samples ofthe proteasome alone did not influence proteasomal activity, its addition to

the reactions containing PSMF1 antagonized the inhibitory effects (part iii, red and blue lines). The subsequent addition of more PSMF1 resulted again in inhibition of proteasomal activity (part iv), which, in turn, ~~again~~ could be reversed by further addition of VCP (not shown). To assess the molar ratios of the reaction mixtures, proteins were precipitated at the end of the experiments. Analysis by SDS-PAGE showed that the observed effects of PSMF1 and VCP on the proteasomal activity are stoichiometric (ah: at which ratio?) (Fig. 3D).

We recently reported on an autophagy-deficient strain (ATG9KO) of the model organism *Dictyostelium discoideum* (Arhzaouy et al., 2012), which has an intrinsic and severe defect of proteasomal activity. To assess whether VCP can also influence the proteasomal activity *in vivo*, we over-expressed RFP-tagged VCP in these cells. Here, we found that an approximately 2-fold increase of VCP protein levels (data not shown) fully restored the proteasomal activity (Fig. 3E).

PSMF1 acts as a polymer

It is currently unknown whether the PSMF1-induced inactivation of the proteasome is due to binding of monomeric or polymeric PSMF1 to the 20S core. Therefore, we performed *in silico* analyses, which indicated that multimers of PSMF1 may bind in place of 19S regulatory particles and thus lead to the formation of catalytically inactive $[PSMF1]_n$:20S proteasome complexes. The simulated model shown here assumes n = 7, i.e. a heptameric ring of PSMF1 on top of the 20S proteasome (Fig. 4A); we cannot exclude the possibility of a hexameric PSMF1 assembly on the 20S particle. E~~Moreover, e~~xperimental evidence for PSMF1 multimers comes from clear native PAGE analyses, which~~, however,~~ indicated the formation of trimers, hexamers, and nonamers (Fig. 4B). **Andreas**: Würde *in silico* auch ein PSMF1-Hexamer auf den heptameren PSMA1-7 Ring des 20S Proteasoms

passen? Das ergäbe ein besseres Gesamtbild. ah: hexa- oder heptamer ist denkbar; wir haben aber keine gerechneten modelle fuer ein hexamer. du koenntest den obigen halbsatz mit einfugen um das zu verdeutlichen.

The binding sites between PSMF1 and VCP have ~~also~~ not yet been experimentally established. VCP assembles into hexamers with its ATPase domains forming a central cylinder that is surrounded by the N-terminal CDC48 domains (DeLaBarre & Brunger, 2003). However, based on the structural similarities between PSMF1 and FAFA1-UBX, another VCP binding partner, we performed molecular modelling addressing the PSMF1-VCP interaction. As a result of our *in silico* modelling, the complex of N-PSMF1:~~N-~~VCP-ND1 in Fig. 4C illustrates the putative binding mode of N-PSMF1 (cartoon representation in turquois) with ~~N-~~VCP-ND1 (surface representation with mapped electrostatics in red (negative potential) and blue (positive potential)). This model and the hexameric VCP structure were used to construct the [N-PSMF1:VCP]$_6$ complex (surface representation with PSMF1 in bluish colors and the VCP monomers in orange and green) (Fig. 4C).

Discussion

Beyond a multitude of other functions, VCP has also been attributed an important role in the degradation of poly-ubiquitinated proteins via the proteasome. A knock-down of VCP in HeLa cells led to the accumulation of poly-ubiquitinated proteins (Wojcik et al, 2004). ~~Other~~Recent studies demonstrated that several substrates of the ubiquitin-proteasomal system need VCP and its co-factors in order to be properly processed (Förster et al, 2014; Zhang & Ye, 2014). Moreover, VCP was detected in proteasomal purifications (Besche et al, 2009; Dai et al, 1998; Guerrero et al, 2008; Shibatani et al, 2006), and a more recent study demonstrated

that VCP associated with the 19S sub-complex of the proteasome upon proteasomal inhibition or over-expression of VCP. This study also indicated that the VCP co-factors Ufd1 and Npl4 promote an enrichment of VCP at the inhibited proteasome (Isakov & Stanhill, 2011).

PSMF1 on the other hand was generally described as a potent inhibitor of proteasomal activity (Cho-Park & Steller, 2013; Chu-Ping et al, 1992; McCutchen-Maloney et al, 2000; Zaiss et al, 1999). In contrast, a recent study suggested that the situation may be more complex as ADP-ribosylated PSMF1 may stimulate proteasomal activity (Cho-Park & Steller, 2013). This latter mechanism relies on abolished binding of the post-translationally modified PSMF1 to the 20S proteasome core, which instead binds and sequesters 19S assembly chaperones, thus liberating 19S regulatory particles for the formation of catalytically active 26S proteasomes. However, this suggestion has been challenged by the findings that the ribosylation inhibitor XAV939 did not decrease proteasomal activity, and that ADP-ribosylation of PSMF1 could not be detected by immunoblotting (Li et al, 2014).

Based on our experimental work in conjunction with *in silico* modelling, we delineate an extended mechanism of proteasome regulation, in which PSMF1 and VCP antagonistically regulate proteasomal activity (Fig. 5). The catalytically active 26S proteasome (top) continually assembles and disassembles (transition 1) *in vivo* into the 20S core particle and the 19S regulatory complex. Only the “free” 20S proteasome seems to interact with PSMF1 (transition 2), as a recent study showed that PSMF1 was able to suppress the assembly of 26S proteasome from 19S and 20S particles, but had no effect on preformed 26S proteasome *in vitro* (Li et al, 2014). The catalytically inactive state of the proteasome is the $[PSMF1]_{7n}$:20S complex (bottom). As previously proposed (McCutchen-Maloney et al, 2000), PSMF1 molecules may indeed act as caps of the 20S proteasomes with the C-terminal

regions of the PSMF1 monomers blocking the entry of substrates to the proteolytically active sites inside the 20S core particle. This PSMF1-mediated inactivation of the proteasome can be counteracted by increasing levels of VCP. VCP assembles into hexamers with its ATPase domains forming a central cylinder that is surrounded by the N-terminal CDC48 domains (DeLaBarre & Brunger, 2003). In our mechanistic model, VCP sequesters PSMF1 from the $[PSMF1]_{7n}$:20S complex and~~,~~ ~~according to our *in silico* analyses,~~ gives rise to $[PSMF1:VCP]_6$ complexes (transition 3). This finally enables the re-assembly of catalytically active 26S proteasomes from "free" 20S core and 19S regulatory particles (transition 4).

We thus propose that in addition to its postulated role ~~in~~of extracti~~n~~gon and shuttling of poly-ubiquitinated proteins ~~and shuttling them to the proteasome~~ (Braun et al, 2002; Raasi & Wolf, 2007), VCP activates the proteasome by counteracting the inhibitory effect of PSMF1. Importantly, our model does not exclude activation of the proteasome by ADP-ribosylation of PSMF1 (Cho-Park & Steller, 2013). Both regulatory mechanisms would lead to re-assembly and activation of the 26S proteasome and facilitate the turnover of degradation-prone proteins. Our data thus provide novel, fundamental insights into the basic regulation of proteasomal activity.

Materials and Methods

Lumier technique

The luminescence-based mammalian interactome mapping (Lumier) technique allows detection and quantitation of protein-protein interactions in mammalian cells (Barrios-Rodiles et al, 2005). The method is based on a double-transfection with plasmids coding for the proteins of interest with either a Renilla luciferase or a Protein A tag. PCR amplified cDNAs of proteins of interest (for details

on primer design and PCR conditions please contact the corresponding authors) were cloned into the pDONR207 vector (Invitrogen) to generate the respective pENTR207 entry vectors of the Gateway cloning/recombination system (Invitrogen). The latter were used to transfer the cDNAs into the Gateway plasmids of the Lumier system (pDEST-RLuc, pDEST-ProtA). The original protocol of the Lumier technique was modified, optimized, and used as follows.

Cell seeding: 293TN cells (BioCat/SBI LV900A-1) were seeded into 6-well-plates and used for transfections on the next day.

Cell transfection: 2 µg of each of the two plasmids, for example pDestLuc-VCP and pDestProtA-PSMF1, were mixed and diluted in 150 µl growth medium lacking serum and antibiotics, and subsequently mixed with 150 µl medium containing 5 µl Lipofectamine (Invitrogen), and incubated for 20 min at room temperature. The transfection mixtures were added to the cells after one washing step with PBS and the addition of 2 ml growth medium, and cells were incubated for 48 h at 37°C and 5% CO_2.

Cell lysis: After removal of the medium, cells were washed two times with PBS and separated from the plastic surface by force pipetting in 1 ml PBS. 500 µl of the cell suspensions were transferred into 1.5 ml reaction tubes, spun down at 3,400 xg for 5 min at 4°C, and kept on ice; the remaining volumes of the cells were used for Protein A immunoblotting. The cell pellets were lysed in 50 µl lysis buffer (22 mM Tris, 1.1% Triton X-100, 275 mM NaCl, 11 mM EDTA, protease inhibitor cocktail (1:50, Sigma), phosphatase inhibitor (1:50, Roche), 1 mM DTT, pH adjusted to 8.0) for 1 h on ice before the suspensions were centrifuged at 16,000 xg for 20 min.

Measurement of input luciferase activity: 10 µl of the cell lysis supernatants were mixed with 40 µl PBS in wells of white flat-bottom non-treated polystyrene microtiter plates (Nunc # 236105) prior to the addition of 70 µl Renilla assay buffer

(300 mM NaCl, 2 mM Na_2EDTA (pH 8), 60 mM phosphate from KH_2PO_4/K_2HPO_4 (pH 7.5), 0.5 mg/ml BSA, 2.5 µM coelenterazine (dissolved in methanol; PJK # 260350), final buffer pH adjusted to 7.0), and used for measurements of the luminescence signal intensities using an Infinite M1000 plate reader (Tecan) in luminescence acquisition mode with an integration time of 10 s/well and the "blue 1" bandpass filter (370 - 480 nm).

Pull-down and measurement of luciferase activity: 5 µl magnetic beads coated with immunoglobulins (Dynabeads M-280 sheep anti-rabbit IgG, Invitrogen # 112-03D) per well were washed twice with PBS and once with lysis buffer, and subsequently mixed with 40 µl of the cell lysis supernatants, which had been transferred into PCR tubes, and incubated for 1 h at 4°C using a rotation device. Beads were then collected using a tube rack with permanent magnets, the supernatants were discarded, and the beads washed four times with PBS. Finally, they were re-suspended in 20 µl PBS, transferred into the white flat-bottom microtiter plates, and the luminescence signal intensities were determined as outlined above.

Proteasomal activity assays

In this study, the chymotrypsin-like proteasomal activity was monitored based on the cleavage of succinyl-LLVY-aminoluciferin. In a secondary reaction, released aminoluciferin is processed by the firefly luciferase and used for luminometry. This luminescence-based technique has the experimental advantage that it allows a direct determination of the proteasomal activity during the entire course of the experiment. In contrast, the commonly used fluorescence-based assay detects the increment of the 7-amino-4-methylcoumarin cleavage product thus limiting the measurement to the initial state.

Proteasome preparations: Human 26S proteasome preparations were derived from HEK293 cells (BostonBiochem, E-365-025) and red blood cells (Enzo Life Sciences, BML-PW9310) and were used for the assays shown in Fig. 3B. Note, that these commercially available preparations of 26S proteasome contained a variable, but significant amount of 20S proteasome as determined by native PAGE. These preparations did neither contain VCP nor PSMF1 as determined by SDS-PAGE and immunoblotting. Own human 20S proteasome was prepared from 293TN cells by digitonin permeabilization in 50 mM Tris/HCl pH 7.5, 250 mM sucrose, 5 mM $MgCl_2$, 2 mM ATP (freshly added), 1 mM DTT (freshly added), 0.5 mM EDTA, 0.025% digitonin, which was followed by ultracentrifugation at 200,000 xg for 2.5h and solubilization of the glassy pellet in the same buffer lacking digitonin according to (Kisselev & Goldberg, 2005). The quality of these proteasome preparations was also verified by native PAGE and immunoblotting. In addition, the presence of all fourteen alpha and beta subunits was verified by mass spectrometry. While all 20S proteasome preparations were free of PSMF1, some contained small amounts of co-purifed VCP hexamers. When 20S proteasome of such a preparation was used for an experiment as shown in Fig. 3C higher amounts of PSMF1 were needed for the inhibition of proteasomal activity.

Proteasomal activities of lysates of murine skeletal muscle and purified proteasome: Proteasomal activity in skeletal muscle tissue lysates as shown in Figs. 2D and 3A was determined according to (Strucksberg et al, 2010). The same protocol was used with 100 ng of human 26S proteasome preparations (either BostonBiochem E-365-025 or Enzo Life Sciences BML-PW9310) as shown in Fig. 3B. The luminescence signals were detected using an Infinite M1000 plate reader (Tecan, Switzerland) in luminescence acquisition mode without any filter and with an integration time of 1 s.

Kinetics of proteasomal activity using purified proteasome, VCP and PMSF1:

For experiments as shown in Figs. 3C and D, in reaction tubes (1.5 ml polypropylene micro tubes, Sarstedt # 72.690.001) samples of 30 µl starting volumes containing 100 ng of human 20S proteasome (either EnzoLifeSciences BML-PW9310, supplied as 1 mg/ml stock in 10 mM Tris/HCl pH 7.0, 25 mM KCl, 1.1 mM $MgCl_2$, 0.1 mM EDTA, 1 mM DTT, 1 mM NaN_3, 2 mM ATP, 35% glycerol, which was diluted 1:100 in 1x concentrated proteasome buffer containing 50 mM Tris/HCl pH 7.4, 40 mM KCl, 5% glycerol, 5 mM $MgCl_2$, 0.5 mM ATP (freshly added), 1 mM DTT (freshly added), 50 µg/ml BSA (freshly added) in our experiments, or alternatively own 20S proteasome derived from 293TN cells as described above) were incubated with human recombinant, tag-free VCP (expression and purification from *E. coli*, cleavage of GST-tag, and protein verification by mass spectrometry according to (Clemen et al, 2010); clear native PAGE was performed to confirm hexamer formation; protein eluted in 50 mM Tris/HCl pH 7.4, 150 mM NaCl, 1 mM DTT, 2 mM ATP, 2 mM $MgCl_2$; doses of 1 µg were used) and/or human PSMF1 (either purchased protein with C-terminal FLAG-tag purified from HEK293 cells (BioCat/Origene TP318938; stock in 10% glycerol, 100 mM glycine, 25 mM Tris/HCl pH 7.3) or alternatively own recombinant protein with N-terminal GST-tag purified from *E. coli* in buffer 50 mM Tris/HCl pH 7.4, 150 mM NaCl, 1 mM DTT; doses of 1 µg were used), or appropriate volumes of the two different buffers for control for 10 minutes at room temperature. Reaction volumes were then increased to 60 µl by the addition of a partially 4x concentrated proteasome buffer (50 mM Tris-HCl, pH 7.4, 160 mM KCl, 20% glycerol, 5 mM $MgCl_2$, 2 mM ATP, 4 mM DTT, 200 µg/ml BSA (10 mg/ml stock, Promega R396E)), transferred into wells of white flat-bottom non-treated polystyrene microtiter plates (Nunc # 236105), and finally increased to 110 µl by the addition of 50 µl of the substrate mixture (Proteasome-Glo Chymotrypsin-Like Assay containing

Suc-LLVY-aminoluciferin, Promega G8622). Luminescence signals were monitored every minute at 37°C in a pre-warmed Infinite M1000 plate reader (Tecan) using the luminescence setup without any filter and with an integration time of 1 s. The reactions with the 20S proteasome alone or in the presence of 30 µM of the highly effective proteasomal inhibitor AdaAhx$_3$L$_3$VS (adamantane-acetyl-(6-aminohexanoyl)$_3$-(leucinyl)$_3$-vinyl-(methyl)-sulfone, Calbiochem; 15 mM stock in DMSO) served as reference and control, respectively. To all reactions that did not contain AdaAhx$_3$L$_3$VS the appropriate volume of DMSO was added.

Experimental notes of caution: The choice of method is crucial for the sensitivity and reproducibility of proteasomal activity measurements. In agreement with a recently published study (Cui et al, 2014), we also noticed that the luminescence intensity values of the proteasomal activity strongly depended on the type of microtiter plate. Moreover, we also observed that the presence of BSA (not pre-coating of the wells, but its presence in the buffer) is mandatory to obtain high levels of proteasomal activity; the requirement of BSA or alternatively soybean trypsin inhibitor has been described previously (Kisselev & Goldberg, 2005).

Molecular modelling

Rigid body docking of N-PSMF1 (PDB entry 2VT8) to the 20S proteasome (PDB entry 1YAU) and VCP-ND1 (PDB entry 3QQ8) was carried out manually using the graphics program O (Jones et al, 1991) to obtain reasonable binding poses without steric clashes. The structure of FAFA1-UBX in complex with the VCP-ND1 domain (PDB entry 3QQ8) served as a template for the manual docking of N-PSMF1 (PDB entry 2VT8), ~~as~~since N-PSMF1 and FAFA1-UBX both possess a central four-/five-stranded β-sheet with protruding loops on one side and flanking α-helices on the other. The initial complexes of N-PSMF1:VCP-ND1 and [N-PSMF1]$_7$:20S

complexes were then subjected to molecular dynamics simulations with Gromacs (Van Der Spoel et al, 2005). The G43a1 force field and the spc water model were used. To ensure a charge-neutral cell, sodium or chloride counter ions were added by replacing solvent molecules at sites of high electrostatic potential. A position-restrained dynamics simulation of 20 ps was performed to equilibrate the solvated protein complexes and gradually heat the simulation cell to 300 K. Periodic boundary conditions were applied in all three dimensions with the Particle Mesh Ewald (PME) method being used to treat the long-range electrostatic interactions. Analyses were performed with Gromacs tools.

Miscellaneous methods

Expression of human GST-VCP in *E. coli*, purification, cleavage of the GST-tag, protein verification, as well as pull-down experiments were performed as described (Clemen et al, 2010). Expression and purification of human GST-PSMF1 from pReceiver-B05 containing the PSMF1 sequence BC126462.1 (with Cys36; GeneCopoeia EX-K2773-B05) or pReceiver-B06 containing sequence NM_006814 (with Phe36; GeneCopoeia EX-A3099-B06) was done accordingly, however, without tag cleavage and with additional dialysis against buffer 50 mM Tris/HCl pH 7.4, 150 mM NaCl, 1 mM DTT. **Maki:** pre-casted gels, buffer, running conditions, marker, staining, etc. for clear-native PAGE. Quantitative real-time PCR (Farbrother et al, 2006) and immunoblotting (Chopard et al, 2000) were done as described. Briefly, snap frozen murine skeletal muscle tissue was pulverized, homogenized in lysis buffer (5 mM Tris, 10% SDS, 0.2 M DTT, 1 mM EDTA, pH 6.8), boiled at 95°C for 5 min, and the lysate was clarified by centrifugation. For gel electrophoresis, 10 µl of the lysate were mixed with 40 µl 1x SDS-sample buffer and boiled again before

loading. Generation of mice haploinsufficient for VCP is described in the legend to Figure S1.

Antibodies used were: VCP, mouse mAb K76-318-1 (Clemen et al, 2010), dilution 1:3,000; PSMF1, goat pAb, Sigma SAB2500788, 1:500; 20S, mouse mAb anti-α1,2,3,5,6,7 subunits, Upstate # 04-038, 1:1,000; 19S, rabbit pAb anti-26S protease regulatory subunit 4 (PSMC1, component of 19S particle), Calbiochem # 539167, 1:1,000; ubiquitin, mouse mAb P4D1, Cell Signaling Technology # 3936, 1:1,000; GAPDH, mouse mAb GAPDH-71.1, Sigma G8795, 1:10,000.

Acknowledgements

Grant support by the German Research Foundation (DFG) within the framework of the multi-location research group FOR1228 (grants CL 381/3-2 to CSC, HA 2092/23-2 to FGH, RO 2173/4-2 to WR, JU 2859/1-2 to SJ, EI 399/7-2 to LE, and SCHR 562/9-2 to RS) and for individual research projects (grants CL 381/1-1 to CSC and SCHR 562/7-1 to RS), by the Fritz-Thyssen-Foundation (grant 10.07.1.165 to RS and CSC), the Australian Research Council (ARC) (grant LE120100071 to AH), and by the Interdisciplinary Center for Clinical Research (IZKF) of the Clinical Center Erlangen (to MT) is gratefully acknowledged.

CSC and RS jointly conceived the study and reviewed all data. CSC and MM conceived and carried out experiments and analyzed data. KHS, JB, LG, LW, FC, KT, JS, JM, and KK carried out experiments and analyzed data. RS, FGH, SJ, and LE conceived experiments and analyzed data. MT, WR, and IB analyzed data. AH performed the *in silico* analyses. CSC and RS wrote the manuscript and prepared the figures. All authors had final approval of the submitted and published versions. The authors declare no conflicts of interests.

We thank Carolin Berwanger and Maria Stumpf for excellent technical assistance. Ufd1 and Npl4 expression plasmids were kindly provided by Annett Böddrich (Max Delbrück Center for Molecular Medicine, Berlin, Germany) and Hemmo Meyer (University of Duisburg-Essen, Germany), respectively. pDEST-RLuc (originally named pcDNA3-Rluc-GW) and pDEST-ProtA (originally named pTREX-Dest30-ProtA) vectors for the Lumier experiments were generously provided by Manfred Kögl (Preclinical Target Development, and Genomics and Proteomics Core Facilities, DKFZ, Heidelberg, Germany).

Competing Interests

The authors declare no conflicts of interests.

References

Arhzaouy K, Strucksberg KH, Tung SM, Tangavelou K, Stumpf M, Faix J, Schroder R, Clemen CS, Eichinger L. 2012. Heteromeric p97/p97(R155C) Complexes Induce Dominant Negative Changes in Wild-Type and Autophagy 9-Deficient Dictyostelium strains. *PLoS One* **7**:e46879.

Baek GH, Cheng H, Choe V, Bao X, Shao J, Luo S, Rao H. 2013. Cdc48: A Swiss Army Knife of Cell Biology. *J Amino Acids* **2013**:183421.

Barrios-Rodiles M, Brown KR, Ozdamar B, Bose R, Liu Z, Donovan RS, Shinjo F, Liu Y, Dembowy J, Taylor IW, Luga V, Przulj N, Robinson M, Suzuki H, Hayashizaki Y, Jurisica I, Wrana JL. 2005. High-throughput mapping of a dynamic signaling network in mammalian cells. *Science* **307**:1621-5.

Besche HC, Haas W, Gygi SP, Goldberg AL. 2009. Isolation of mammalian 26S proteasomes and p97/VCP complexes using the ubiquitin-like domain from HHR23B reveals novel proteasome-associated proteins. *Biochemistry* **48**:2538-49.

Braun S, Matuschewski K, Rape M, Thoms S, Jentsch S. 2002. Role of the ubiquitin-selective CDC48(UFD1/NPL4)chaperone (segregase) in ERAD of OLE1 and other substrates. *EMBO J* **21**:615-21.

Cho-Park PF, Steller H. 2013. Proteasome regulation by ADP-ribosylation. *Cell* **153**:614-27.

Chopard A, Pons F, Charpiot P, Marini JF. 2000. Quantitative analysis of relative protein contents by Western blotting: comparison of three members of the dystrophin-glycoprotein complex in slow and fast rat skeletal muscle. *Electrophoresis* **21**:517-22.

Chu-Ping M, Slaughter CA, DeMartino GN. 1992. Purification and characterization of a protein inhibitor of the 20S proteasome (macropain). *Biochim Biophys Acta* **1119**:303-11.

Clemen CS, Tangavelou K, Strucksberg KH, Just S, Gaertner L, Regus-Leidig H, Stumpf M, Reimann J, Coras R, Morgan RO, Fernandez MP, Hofmann A, Muller S, Schoser B, Hanisch FG, Rottbauer W, Blumcke I, von Horsten S, Eichinger L, Schröder R. 2010. Strumpellin is a novel valosin-containing protein binding partner linking hereditary spastic paraplegia to protein aggregation diseases. *Brain* **133**:2920-41.

Cui Z, Gilda JE, Gomes AV. 2014. Crude and purified proteasome activity assays are affected by type of microplate. *Anal Biochem* **446**:44-52.

Dahlmann B. 2005. Proteasomes. *Essays Biochem* **41**:31-48.

Dai RM, Chen E, Longo DL, Gorbea CM, Li CC. 1998. Involvement of valosin-containing protein, an ATPase Co-purified with IkappaBalpha and 26 S proteasome, in ubiquitin-proteasome-mediated degradation of IkappaBalpha. *J Biol Chem* **273**:3562-73.

de Bot ST, Schelhaas HJ, Kamsteeg EJ, van de Warrenburg BP. 2012. Hereditary spastic paraplegia caused by a mutation in the VCP gene. *Brain* **135**:e223.

DeLaBarre B, Brunger AT. 2003. Complete structure of p97/valosin-containing protein reveals communication between nucleotide domains. *Nat Struct Biol* **10**:856-63.

Farbrother P, Wagner C, Na J, Tunggal B, Morio T, Urushihara H, Tanaka Y, Schleicher M, Steinert M, Eichinger L. 2006. Dictyostelium transcriptional host cell response upon infection with Legionella. *Cell Microbiol* **8**:438-56.

Förster F, Schuller JM, Unverdorben P, Aufderheide A. 2014. Emerging mechanistic insights into AAA complexes regulating proteasomal degradation. *Biomolecules* **4**:774-94.

Frohlich KU, Fries HW, Rudiger M, Erdmann R, Botstein D, Mecke D. 1991. Yeast cell cycle protein CDC48p shows full-length homology to the mammalian protein VCP and is a member of a protein family involved in secretion, peroxisome formation, and gene expression. *J Cell Biol* **114**:443-53.

Gomes AV. 2013. Genetics of Proteasome Diseases. *Scientifica (Cairo)* **2013**:637629.

Guerrero C, Milenkovic T, Przulj N, Kaiser P, Huang L. 2008. Characterization of the proteasome interaction network using a QTAX-based tag-team strategy and protein interaction network analysis. *Proc Natl Acad Sci U S A* **105**:13333-8.

Isakov E, Stanhill A. 2011. Stalled proteasomes are directly relieved by P97 recruitment. *J Biol Chem*

Jankowska E, Stoj J, Karpowicz P, Osmulski PA, Gaczynska M. 2013. The proteasome in health and disease. *Curr Pharm Des* **19**:1010-28.

Johnson JO, Mandrioli J, Benatar M, Abramzon Y, Van Deerlin VM, Trojanowski JQ, Gibbs JR, Brunetti M, Gronka S, Wuu J, Ding J, McCluskey L, Martinez-Lage M, Falcone D, Hernandez DG, Arepalli S, Chong S, Schymick JC, Rothstein J, Landi F, Wang YD, Calvo A, Mora G, Sabatelli M, Monsurro MR, Battistini S, Salvi F, Spataro R, Sola P, Borghero G, Galassi G, Scholz SW, Taylor JP, Restagno G, Chio A, Traynor BJ. 2010. Exome sequencing reveals VCP mutations as a cause of familial ALS. *Neuron* **68**:857-64.

Jones TA, Zou JY, Cowan SW, Kjeldgaard. 1991. Improved methods for building protein models in electron density maps and the location of errors in these models. *Acta Crystallogr A* **47 (Pt 2)**:110-9.

Jung T, Catalgol B, Grune T. 2009. The proteasomal system. *Mol Aspects Med* **30**:191-296.

Kisselev AF, Goldberg AL. 2005. Monitoring activity and inhibition of 26S proteasomes with fluorogenic peptide substrates. *Methods Enzymol* **398**:364-78.

Lamb JR, Fu V, Wirtz E, Bangs JD. 2001. Functional analysis of the trypanosomal AAA protein TbVCP with trans-dominant ATP hydrolysis mutants. *J Biol Chem* **276**:21512-20.

Leon A, McKearin D. 1999. Identification of TER94, an AAA ATPase protein, as a Bam-dependent component of the Drosophila fusome. *Mol Biol Cell* **10**:3825-34.

Li X, Thompson D, Kumar B, DeMartino GN. 2014. Molecular and Cellular Roles of PI31 (PSMF1) Protein in Regulation of Proteasome Function. *J Biol Chem* **289**:17392-405.

McCutchen-Maloney SL, Matsuda K, Shimbara N, Binns DD, Tanaka K, Slaughter CA, DeMartino GN. 2000. cDNA cloning, expression, and functional characterization of PI31, a proline-rich inhibitor of the proteasome. *J Biol Chem* **275**:18557-65.

Müller JM, Deinhardt K, Rosewell I, Warren G, Shima DT. 2007. Targeted deletion of p97 (VCP/CDC48) in mouse results in early embryonic lethality. *Biochem Biophys Res Commun* **354**:459-65.

Raasi S, Wolf DH. 2007. Ubiquitin receptors and ERAD: a network of pathways to the proteasome. *Semin Cell Dev Biol* **18**:780-91.

Rechsteiner M, Hill CP. 2005. Mobilizing the proteolytic machine: cell biological roles of proteasome activators and inhibitors. *Trends Cell Biol* **15**:27-33.

Shibatani T, Carlson EJ, Larabee F, McCormack AL, Fruh K, Skach WR. 2006. Global organization and function of mammalian cytosolic proteasome pools: Implications for PA28 and 19S regulatory complexes. *Mol Biol Cell* **17**:4962-71.

Sorokin AV, Kim ER, Ovchinnikov LP. 2009. Proteasome system of protein degradation and processing. *Biochemistry (Mosc)* **74**:1411-42.

Strucksberg KH, Tangavelou K, Schröder R, Clemen CS. 2010. Proteasomal activity in skeletal muscle: a matter of assay design, muscle type, and age. *Anal Biochem* **399**:225-9.

Van Der Spoel D, Lindahl E, Hess B, Groenhof G, Mark AE, Berendsen HJ. 2005. GROMACS: fast, flexible, and free. *J Comput Chem* **26**:1701-18.

Watts GD, Wymer J, Kovach MJ, Mehta SG, Mumm S, Darvish D, Pestronk A, Whyte MP, Kimonis VE. 2004. Inclusion body myopathy associated with Paget disease of bone and frontotemporal dementia is caused by mutant valosin-containing protein. *Nat Genet* **36**:377-81.

Wojcik C, Yano M, DeMartino GN. 2004. RNA interference of valosin-containing protein (VCP/p97) reveals multiple cellular roles linked to ubiquitin/proteasome-dependent proteolysis. *J Cell Sci* **117**:281-92.

Zaiss DM, Standera S, Holzhutter H, Kloetzel P, Sijts AJ. 1999. The proteasome inhibitor PI31 competes with PA28 for binding to 20S proteasomes. *FEBS Lett* **457**:333-8.

Zhang T, Ye Y. 2014. The final moments of misfolded proteins en route to the proteasome. *DNA Cell Biol* **33**:477-83.

Figure Legends

Figure 1.

VCP directly interacts with PSMF1 (proteasome inhibitor PI31 subunit). A, B, VCP protein interaction analyses using the Lumier-technique, which allows detection and quantitation of direct protein-protein interactions in mammalian cells (Barrios-Rodiles et al, 2005). The analyses are based on a double-transfection with plasmids coding for Renilla luciferase- (Luc) and Protein A- (Prot A) tagged proteins. Negative controls (normalized luminescence signal intensity set to 1, dotted lines, both left columns) are based on the sole transfection of the luciferase-tagged proteins. Statistical significance was calculated by Student's t-test; n indicates the number of independent experiments; error bars indicate standard errors of the mean. **A,** the high normalized luminescence signal intensity of VCP (middle column) reflects its hexamerization state. To visualize the dynamic range of the Lumier method, the luminescence of a coronin protein (CRN2/Coro1C) that forms trimers is shown (right column). **B,** luminescence analyses indicate binding of VCP to PSMF1 with binding strength similar to those of the well-established VCP binding partners Ufd1 and Npl4. Further, the Lumier method showed a lack of interaction of VCP with the 20S proteasome subunit PSMA1. **C,** confirmation of the direct VCP – PSMF1 interaction by pull-down assays employing purified recombinant human VCP (untagged) and PSMF1 (GST-tagged) proteins. Negative controls were GST-PSMA1 and GST alone. Asterisks, degradation products of PSMF1 as determined by mass spectrometry.

Figure 2.

VCP haploinsufficient mice show reduced specific proteasomal activity and increased protein ubiquitination. A, quantitative real-time RT-PCR analyses of VCP mRNA expression in skeletal muscle tissue derived from wild-type (WT) and heterozygous (HET) congenic B6J.129S2-*Vcp*$^{tm1(ko)Cscl\&Rfsr}$ mice. Mean values and standard errors were obtained by four-fold repeated measurements in two animals

per genotype. **B,** densitometric analyses of VCP immunoblots. Mean values and standard errors were calculated by analyzing 25 and 29 bands derived from wild-type and heterozygous mice, respectively. Columns in A and B represent relative values with wild-type expression scaled to 1. *p*-values were calculated by Student's t-test. The reduced levels of VCP mRNA and protein demonstrate a VCP haploinsufficiency. **C,** the reduced VCP protein expression level is associated with increased protein ubiquitination (ubiq; note, this is a pattern of increased ubiquitination levels typical for skeletal muscle), whereas the levels of PSMF1, 19S, and 20S proteasome were unchanged. GAPDH was used as loading control. **D,** luminescence-based proteasomal activity measurements in skeletal muscle tissue from lower hind limbs of three months old mice. The specific proteasomal activity is normalized to the amount of proteasome. Note, that the specific chymotrypsin-like proteasomal activity in VCP haploinsufficient mice is significantly reduced. Mean values and standard errors were obtained from six independent experiments; *p*-values were calculated by Student's t-test; activity of wild-type mice was set to 1.

Figure 3.

VCP and PSMF1: antagonistic regulators of proteasomal activity. A, proteasomal activity of lysates prepared from skeletal muscle tissue derived from VCP haploinsufficient mice increased in a dose dependent manner upon addition of recombinant human VCP purified from bacteria. Mean values and standard errors were obtained from two independent experiments. Columns represent relative values of the normalized chymotrypsin-like activity; proteasomal activity without addition of VCP was set to 1. **B,** corresponding assay using a preparation of human 26S proteasome derived from HEK293 cells showing no VCP-mediated increase of proteasomal activity. **C,** luminescence-based proteasomal activity assays employing

human 20S proteasome derived from red blood cells, proteasomal inhibitor AdaAhx$_3$L$_3$VS, recombinant human VCP purified from bacteria, and recombinant human PSMF1 purified from HEK293 cells were monitored until steady-state was reached (panel (i); y-axis: counts per second). The reactions were continued after the addition of PSMF1 or VCP as indicated by the arrowheads (panels (ii) - (iv); y-axis: normalized activity; activity of 20S alone was used as reference and set to 1). Gaps before the arrowheads indicate a delay of three minutes before measurements were resumed after each protein addition. The data shown were derived from a single continuous experiment that had been independently conducted three times with the same experimental design. Three more experiments with identical results employed 20S proteasome prepared from 293TN cells in conjunction with recombinant human GST-PSMF1 purified from *E coli*. **D,** to visualize the stoichiometry of PMSF1 and VCP used in C, proteins of the reaction mixtures were chloroform-methanol precipitated after completion of the reactions, separated by SDS-PAGE, and stained by Coomassie Brilliant Blue. Since only 100 ng of proteasome were used per reaction, subunits of the proteasome are not visible; the single band at approximately 70 kDa corresponds to BSA present in the proteasome buffer. Contaminations of the purified PSMF1 with bovine actin and tubulin as well as horse Hsp90 are indicated by open circles. Reactions annotated with an asterisk did not receive PSMF1, but contained a BSA fragment of similar size as determined by mass spectrometry. The prominent band at 64 kDa corresponds to the recombinant firefly luciferase (LucLa). Molarities of proteasome, PSMF1, and VCP are indicated. VCP immunoblotting confirmed that the proteasome preparations were free of VCP that may have been co-purified. **E,** *in vivo* rescue of the specific proteasomal activity by over-expression of RFP-tagged VCP in a previously reported *Dictyostelium discoideum* ATG9^{KO} strain, exhibiting a drastically reduced proteasomal activity (Arhzaouy et al, 2012). Activity of

AX2 wild-type cells was set to 1. We previously reported a similar finding (Arhzaouy et al, 2012), however, for the purpose of the present study we had performed three additional measurements to further substantiate the initial finding.

Figure 4.

PSMF1 interactions with 20S proteasome and VCP: a matter of polymers. A, we propose that a PSMF1 ~~hepta~~multimer replaces the 19S regulatory particle and leads to the formation of a catalytically inactive [N-PSMF1]~~7~~n:20S proteasome (for illustration, n = 7). The [N-PSMF1]~~7~~n:20S assembly is based on molecular modelling, for which monomeric N-PSMF1 (PDB entry 2VT8) was first manually docked on the PSMA1-7 ring of the 20S proteasome (PDB entry 1YAU), such that the N-terminal end of N-PSMF1 projects radially to the outside and the C-terminal end into the inner cavity. In a second step, this state of arrangement allowed the formation of a heptameric ring of N-PSMF1 on top of the PSMA1-7 without severe clashes between the individual N-PSMF1 monomers. The resulting assembly was subjected to molecular dynamics simulations and remained stable over the time course of the simulation (t = 10 ns). The putative binding site of an N-PSMF1 monomer (cartoon representation of secondary structure elements) to the PSMA1-7 ring is indicated in green, whereas the binding site to VCP is given in magenta; the latter contains the amino acid sequence LYV which matches an HbYX (hydrophobic residue/tyrosine/other amino acid) motif that is well-known for modulators of proteasomal activity. The amino acid stretch given in yellow represents interaction interfaces with both the proteasome and VCP in our models. **B,** recombinant purified GST-PSMF1 and GST for control were separated by clear-native PAGE and stained by Coomassie brilliant blue. Whereas~~ile~~ GST remains monomeric, PSMF1 forms timers, hexamers, and nonamers. Asterisk, contamination by bacterial GroL, as

determined by mass spectrometry. **C,** molecular modelling addressing the PSMF1-VCP interaction was performed based on the structural similarities between PSMF1 and FAFA1-UBX, another VCP binding partner. N-PSMF1:~~N-~~VCP-ND1 illustrates the potential binding mode of N-PSMF1 (cartoon representation in turquois) with ~~N-~~VCP-ND1 (surface representation with mapped electrostatics in red (negative potential) and blue (positive)). The structure of FAFA1-UBX in complex with VCP-ND1 domain (PDB entry 3QQ8) served as a template for manual docking of N-PSMF1 (PDB entry 2VT8) followed by molecular dynamics simulations to obtain the final binding mode (t = 22.5 ns). This equilibrated model of N-PSMF1:~~N-~~VCP-ND1 and the hexameric VCP structure (PDB entry 1R7R) were used to construct the [N-PSMF1:VCP]$_6$ complex (surface representation with PSMF1 in bluish colors and the VCP monomers in orange and green).

Figure 5.

Model for the antagonistic regulation of proteasomal activity via PSMF1 and VCP. Top, surface representation of the 19S regulatory complex and the 20S core particle (two outer PSMA1-7 and two inner PSMB1-7 rings), which together form the catalytically active 26S proteasome. The surface representation is based on an electron microscopy reconstruction of the 26S proteasome (PDB entry 4C0V). Transition 1, disassembly of the 26S proteasome. Left, “free” 20S core particle after dissociation of the 19S complex. Transition 2, binding of PSMF1 to the 20S proteasome. Bottom, PSMF1 (in bluish colors) induces inactivation of the proteasome via formation of a [N-PSMF1]$_{7n}$:20S proteasome complex. Transition 3, VCP induces the re-activation of the proteasome by sequestration of PSMF1 and formation of an N-PSMF1:VCP hexamer ([N-PSMF1:VCP]$_6$). Right, “free” 20S core

particle after sequestration of PSMF1. Transition 4, reassembly of the catalytically active 26S proteasome from 19S and 20S proteasome complexes.

Supplemental Information

Supplemental Figure 1

VCP gene targeting strategy and verification. To study the pathophysiological consequences of IBMPFD disease causing VCP mutations, we aimed to generate a VCP knock-in mouse model. However, one approach did not lead to the generation of the intended R155C VCP knock-in mice, but resulted in a mouse strain that is haploinsufficient for VCP. This congenic B6J.129S2-*Vcp*$^{tm1(ko)Cscl\&Rfsr}$ mouse model was used for the purpose of the present study. **A,** scheme of the targeting strategy resulting in the knock-in mice at the genomic level. **B,** PCR genotyping employing the indicated primer pair confirms the presence of a knock-in allele with a 337 bp product containing the loxP site in heterozygous mice vs. 267 bp derived from the wild-type allele. **C**, Southern blot verification of heterozygous knock-in mice based on KpnI/SacI restriction digestion and hybridization with an external 5' probe leading to the detection of the expected 5.1 kb knock-in and 9.5 kb wild-type fragments. **D,** verification of the presence of the R155C VCP mutation at the genomic level by sequencing of the above PCR product from heterozygous mice; the chromatogram shows the expected double signal for TGT (Cys) and CGG (Arg) from the knock-in and wild-type alleles, respectively. Note that the sequence is given in reverse complement orientation. **E,** to verify the presence of the mutant VCP mRNA, RT-PCR analysis was performed. The insertion of the R155C VCP mutation destroys an endogenous NciI restriction site thus allowing quantitation of the mutant and wild-type VCP mRNA species. However, the NciI restriction digestion of the 277 bp RT-PCR product resulted in the complete cleavage into two fragments of 156 and 121 bp in both wild-type and heterozygous mice. Though a correct targeting on the genomic level was confirmed, the latter result made it clear that this attempt to generate the

R155C knock-in mouse model failed. **F,** in addition, northern blot analysis of the VCP mRNA from wild-type and heterozygous mice employing a mixture of three probes covering the full-length VCP mRNA showed identical hybridization patterns and no evidence for aberrant VCP mRNA species. The arrowhead indicates the full-length VCP mRNA of 3.9 kb. Various additional RT-PCR as well as immunoblotting experiments using different mono- and polyclonal antibodies directed against N- and C-terminal VCP epitopes demonstrated the sole presence of full-length wild-type VCP mRNA and protein. Based on our data and additional *in silico* analyses we finally concluded that the VCP haploinsufficiency is due to the functional inactivation of the targeted VCP allele. In this setting, the presence of the single remaining loxP site in intron 4 caused aberrant splicing and subsequent nonsense-mediated decay of the R155C mutant VCP mRNA. Note, that in a previous study the heterozygous knock-out of VCP based on the deletion of a genomic region comprising the VCP promoter, transcription start site, and exon 1, did not cause reduction of the VCP protein levels (Müller et al, 2007). In agreement with this previous study demonstrating that the homozygous lack of VCP leads to early embryonic lethality, interbreeding of our animals with one non-functional VCP allele only resulted in the generation of wild-type and heterozygous animals. The mouse model was generated according to our specifications (CSC, RS) by genOway, Lyon, France.

Supplemental References

Müller JM, Deinhardt K, Rosewell I, Warren G, Shima DT. 2007. Targeted deletion of p97 (VCP/CDC48) in mouse results in early embryonic lethality. *Biochem Biophys Res Commun* **354**:459-65.

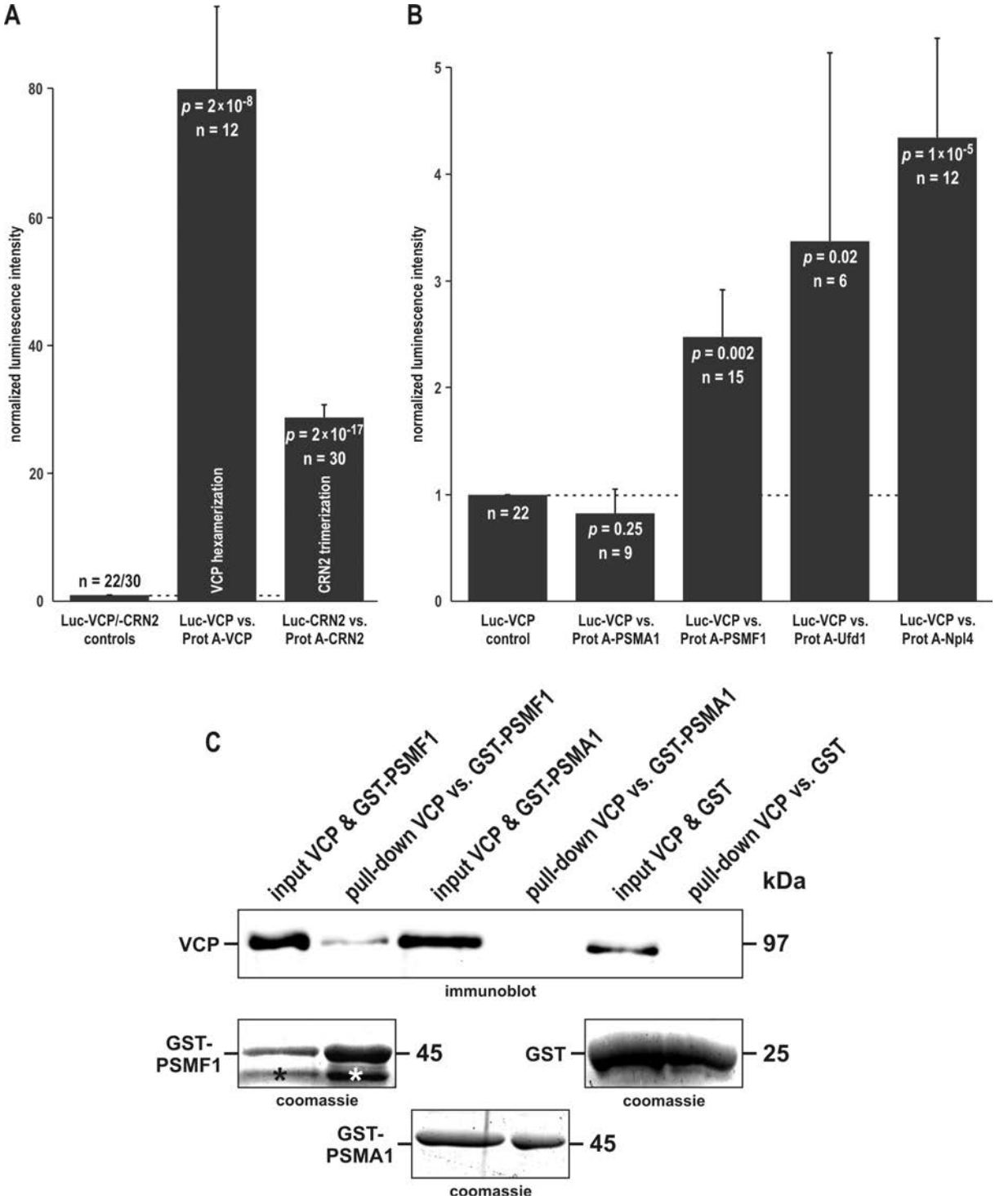
A
normalized luminescence intensity
p = 2×10-8
n = 12
VCP hexamerization
p = 2×10-17
n = 30
CRN2 trimerization
n = 22/30
Luc-VCP/-CRN2 controls
Luc-VCP vs. Prot A-VCP
Luc-CRN2 vs. Prot A-CRN2
B
normalized luminescence intensity
n = 22
p = 0.25
n = 9
p = 0.002
n = 15
p = 0.02
n = 6
p = 1×10-5
n = 12
Luc-VCP control
Luc-VCP vs. Prot A-PSMA1
Luc-VCP vs. Prot A-PSMF1
Luc-VCP vs. Prot A-Ufd1
Luc-VCP vs. Prot A-Npl4
C
input VCP & GST-PSMF1
pull-down VCP vs. GST-PSMF1
input VCP & GST-PSMA1
pull-down VCP vs. GST-PSMA1
input VCP & GST
pull-down VCP vs. GST
kDa
VCP
97
immunoblot
GST-PSMF1
45
coomassie
GST
25
coomassie
GST-PSMA1
45
coomassie

Fig. 1

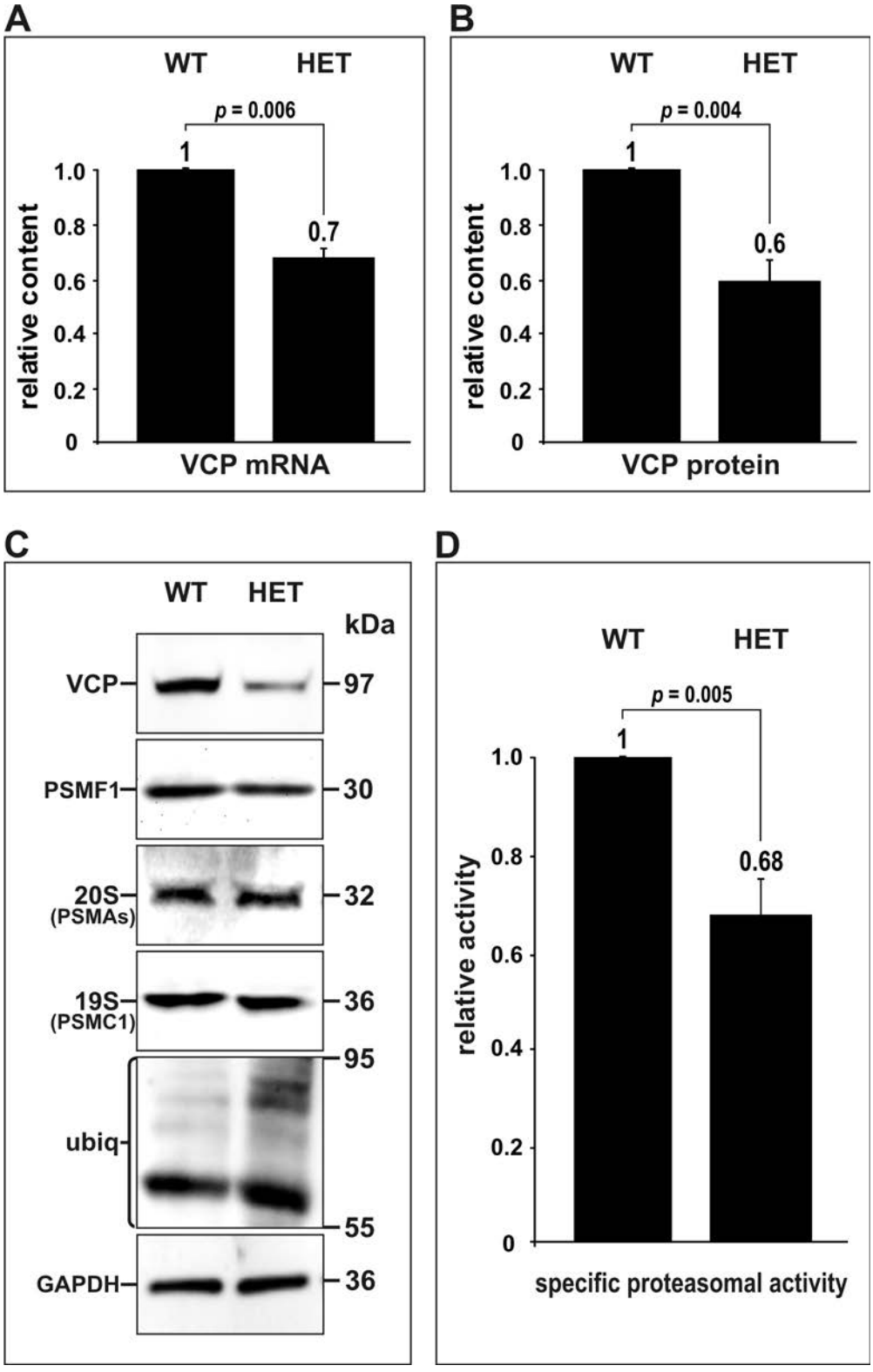
A
WT
HET
p = 0.006
1
0.7
1.0
0.8
0.6
0.4
0.2
0
relative content
VCP mRNA
B
WT
HET
p = 0.004
1
0.6
1.0
0.8
0.6
0.4
0.2
0
relative content
VCP protein
C
WT
HET
kDa
VCP
97
PSMF1
30
20S
(PSMAs)
32
19S
(PSMC1)
36
95
ubiq
55
GAPDH
36
D
WT
HET
p = 0.005
1
0.68
1.0
0.8
0.6
0.4
0.2
0
relative activity
specific proteasomal activity

Fig. 2

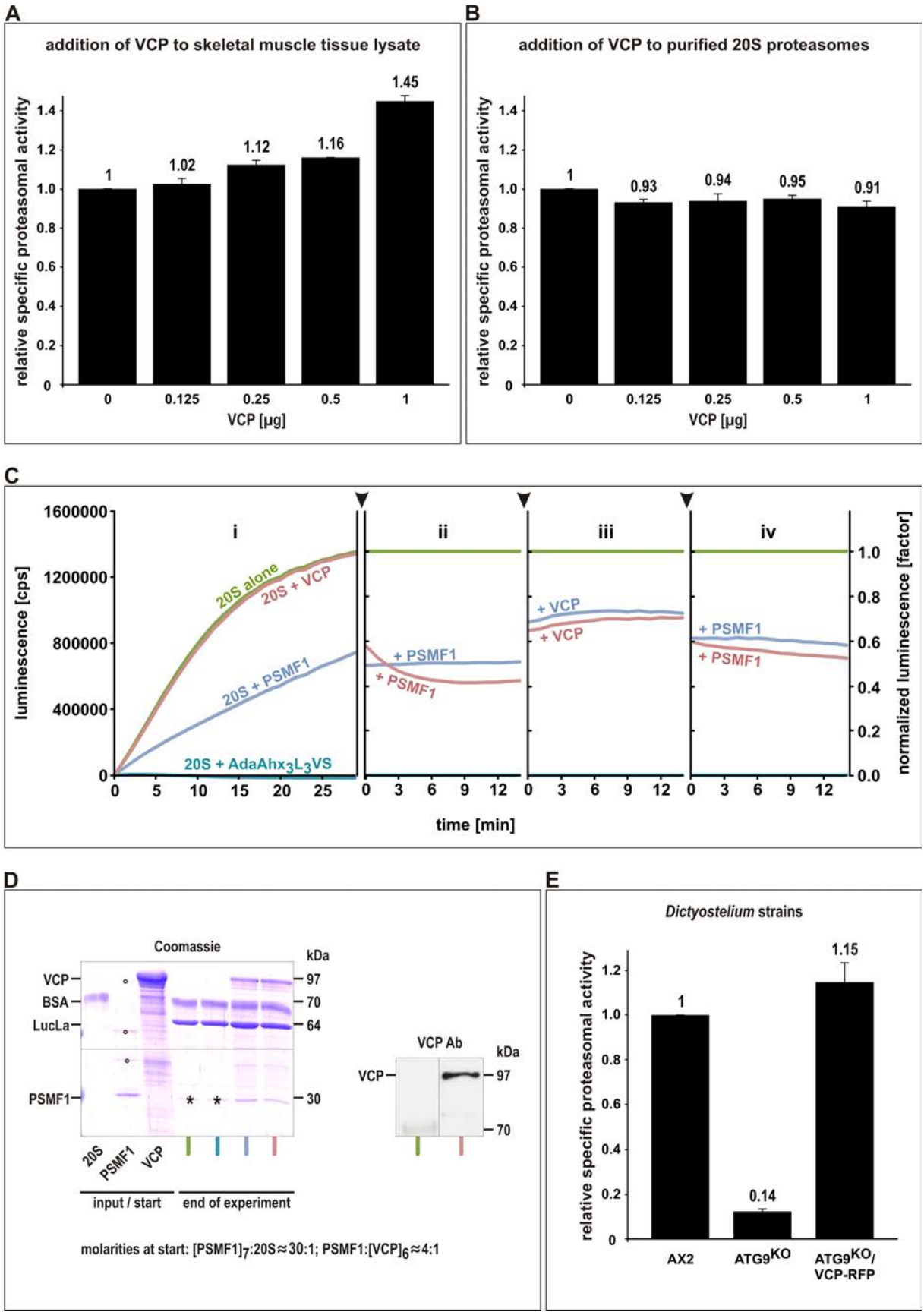
A
addition of VCP to skeletal muscle tissue lysate
relative specific proteasomal activity
1
1.02
1.12
1.16
1.45
0
0.125
0.25
0.5
1
VCP [µg]
B
addition of VCP to purified 20S proteasomes
relative specific proteasomal activity
1
0.93
0.94
0.95
0.91
0
0.125
0.25
0.5
1
VCP [µg]
C
luminescence [cps]
normalized luminescence [factor]
i
ii
iii
iv
20S alone
20S + VCP
20S + PSMF1
20S + AdaAhx3L3VS
+ PSMF1
+ PSMF1
+ VCP
+ VCP
+ PSMF1
+ PSMF1
time [min]
D
Coomassie
kDa
VCP
BSA
LucLa
PSMF1
97
70
64
30
20S
PSMF1
VCP
input / start
end of experiment
VCP Ab
kDa
VCP
97
70
molarities at start: [PSMF1]7:20S≈30:1; PSMF1:[VCP]6≈4:1
E
Dictyostelium strains
relative specific proteasomal activity
1
0.14
1.15
AX2
ATG9KO
ATG9KO/
VCP-RFP

Fig. 3

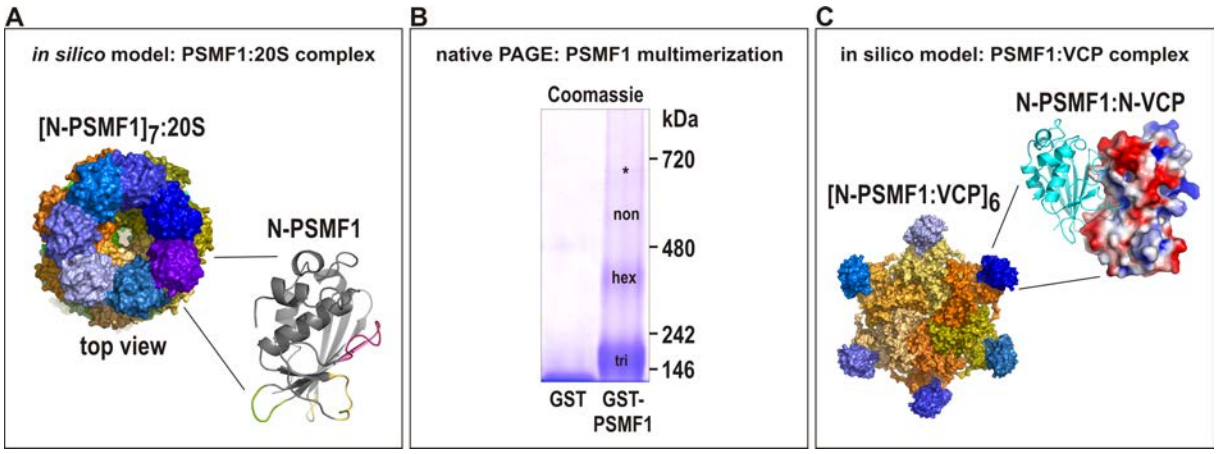
A
in silico model: PSMF1:20S complex
[N-PSMF1]7:20S
N-PSMF1
top view
B
native PAGE: PSMF1 multimerization
Coomassie
kDa
720
480
242
146
*
non
hex
tri
GST
GST-PSMF1
C
in silico model: PSMF1:VCP complex
N-PSMF1:N-VCP
[N-PSMF1:VCP]6

Fig. 4

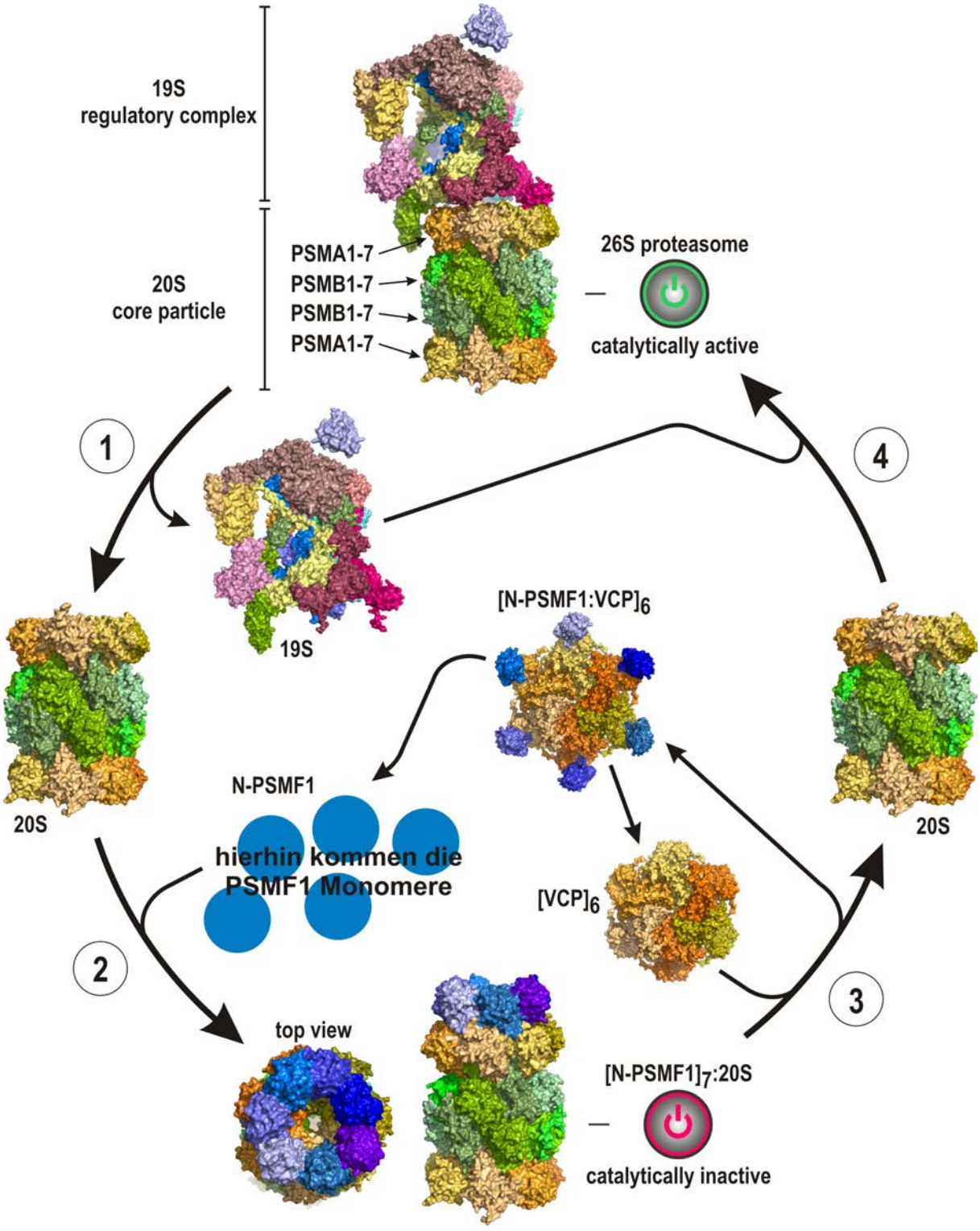
19S
regulatory complex
20S
core particle
PSMA1-7
PSMB1-7
PSMB1-7
PSMA1-7
26S proteasome
catalytically active
1
19S
20S
[N-PSMF1:VCP]6
N-PSMF1
hierhin kommen die
PSMF1 Monomere
[VCP]6
2
3
4
20S
top view
[N-PSMF1]7:20S
catalytically inactive

Fig. 5

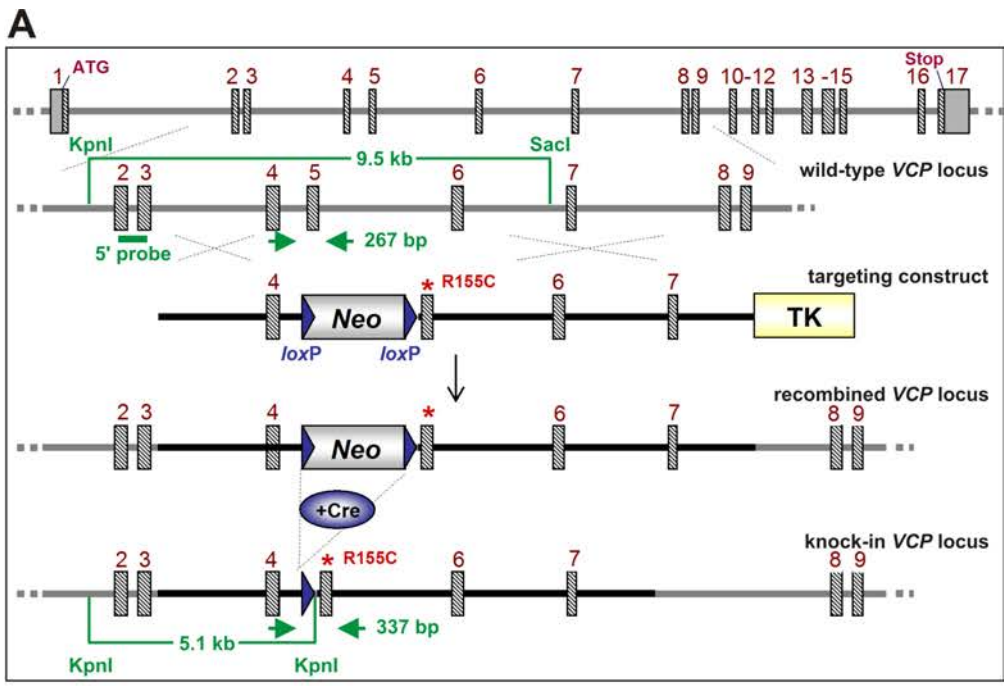
A
1 ATG
2 3
4 5
6
7
8 9
10-12
13 -15
Stop
16 17
KpnI
SacI
9.5 kb
wild-type VCP locus
5' probe
267 bp
targeting construct
R155C
Neo
TK
loxP
loxP
recombined VCP locus
+Cre
knock-in VCP locus
337 bp
5.1 kb
KpnI
KpnI

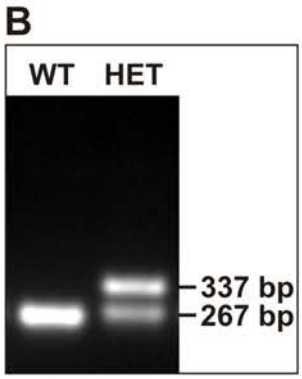
B
WT HET
337 bp
267 bp

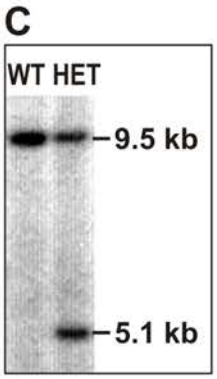
C
WT HET
9.5 kb
5.1 kb

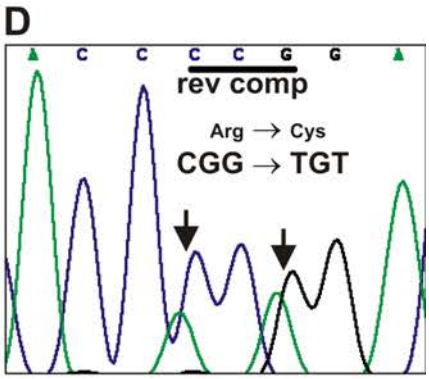
D
C C C C G G
rev comp
Arg → Cys
CGG → TGT

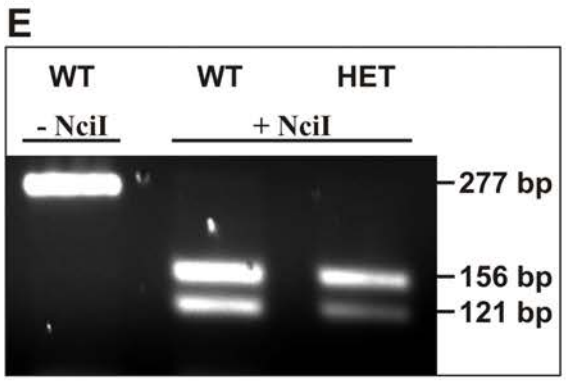
E
WT
WT
HET
- NciI
+ NciI
277 bp
156 bp
121 bp

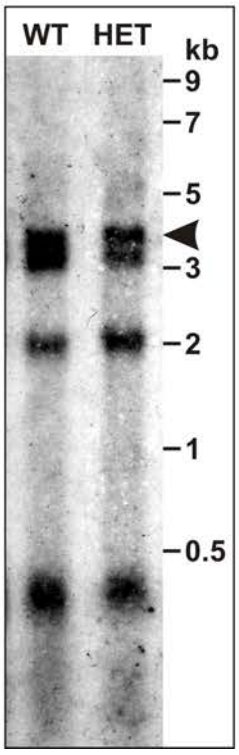
F
WT HET
kb
9
7
5
3
2
1
0.5